LBL-23190
Preprint

Lawrence Berkeley Laboratory
UNIVERSITY OF CALIFORNIA

RECEIVED
BERKELEY LABORATORY
MAY 12 1987
LIBRARY AND
DOCUMENTS SECTION

Submitted to Physical Review C

INTERACTION ENERGY IN INFINITE NUCLEAR MATTER IN THE HYBRID SOLITON MODEL

D. Hahn and N.K. Glendenning

March 1987

TWO-WEEK LOAN COPY
This is a Library Circulating Copy
which may be borrowed for two weeks.

NUCLEAR SCIENCE DIVISION

LBL-23190 c.2

Prepared for the U.S. Department of Energy under Contract DE-AC03-76SF00098

DISCLAIMER

This document was prepared as an account of work sponsored by the United States Government. While this document is believed to contain correct information, neither the United States Government nor any agency thereof, nor the Regents of the University of California, nor any of their employees, makes any warranty, express or implied, or assumes any legal responsibility for the accuracy, completeness, or usefulness of any information, apparatus, product, or process disclosed, or represents that its use would not infringe privately owned rights. Reference herein to any specific commercial product, process, or service by its trade name, trademark, manufacturer, or otherwise, does not necessarily constitute or imply its endorsement, recommendation, or favoring by the United States Government or any agency thereof, or the Regents of the University of California. The views and opinions of authors expressed herein do not necessarily state or reflect those of the United States Government or any agency thereof or the Regents of the University of California.

LBL-23190

Interaction Energy in Infinite Nuclear Matter in the Hybrid Soliton Model [1]

Detlev Hahn and Norman K. Glendenning

Nuclear Science Division
Lawrence Berkeley Laboratory
University of California
Berkeley, California 94720

March 27, 1987

Abstract:

The hybrid soliton model describes nucleons as consisting of quarks and pion and sigma meson fields. We place these nucleons on a three-dimensional lattice and calculate the dependence of the total energy on the density. Various higher order terms in the meson fields are implemented into the Lagrangian of the model to change the behaviour of the interaction energy between the nucleons. Due to the increase in quark kinetic energy at higher densities we have not been able to obtain a minimum at ground state nuclear density.

[1] Work supported by the Director, Office of High Energy and Nuclear Physics of the Department of Energy under Contract DE-AC03-76SF00098.

1. Introduction

Since t'Hooft [1] and Witten [2] showed the equivalence of QCD to an effective meson theory in the limit of large N (number of colors), many authors have worked on models which describe the nucleon in terms of meson fields only [3]. Special interest focused on Skyrme's old soliton solution [4]; it was demonstrated that it resembles the nucleon in properties like the magnetic moment, the charge radius and the axial coupling constant [5] and that quantized solutions may carry spin 1/2 [5,6]. It's resonance states in pion-skyrmion scattering agree with the nuclear spectrum at the 30% level [7]. The effective Lagrangian of the Skyrme model is very simple and has served as a starting point for more complicated soliton models of the nucleon like the present one.

The introduction of the chirally invariant oxhybrid soliton model by Kahana, Ripka and Soni [8] and Birse and Banerjee [9] brought a new aspect into the discussion of solitons. Quarks were explicitly introduced and coupled to the meson fields without being confined by an artificial bag. In previous papers [10], [11] this model was used to describe nuclear matter by placing the solitons on a cubic lattice. A transition mechanism from a phase with the quarks 'confined' (or deeply bound) to one where quarks could move freely through the lattice was obtained [10].

However, a serious shortcoming of this description was the behaviour of the interaction energy between the solitons. It would rise from zero at large soliton separations to $\sim$ 600 MeV at one fermi. In this paper we try to address this problem by introducing higher order terms in the chiral meson fields into the Lagrangian of the model.

2. Lagrangian

We start with the Lagrangian used in ref. [10] for the hybrid soliton model, consisting of a kinetic energy term in the classical $(\sigma, \vec{\pi})$ meson fields

$$\mathcal{L}_1 = -\frac{f_\pi^2}{4} Tr\left\{U^\dagger \partial_\mu U\, U^\dagger \partial^\mu U\right\} = \frac{1}{2}\left[\partial_\mu \sigma \partial^\mu \sigma + \partial_\mu \vec{\pi} \partial^\mu \vec{\pi}\right] \tag{2.1}$$

and the Lagrangian of free quarks, Yukawa coupled to the $\sigma, \vec{\pi}$ mesons:

$$\mathcal{L}_2 = \bar{\Psi}\left[i\gamma_\mu \partial^\mu - g(\sigma + i\gamma_5 \vec{\tau}\cdot\vec{\pi})\right]\Psi \tag{2.2}$$

$\hbar c$ is set equal to 1. The matrix U depends on the meson degrees of freedom

$$U = \frac{1}{f_\pi}\left(\sigma(\vec{r}) + i\vec{\tau}\cdot\vec{\pi}(\vec{r})\right) \tag{2.3}$$

The coupling constant, g, can be adjusted to yield the nucleon mass of $\sim$ 940 MeV for the soliton. The pion decay constant is denoted by $f_\pi = 93$ MeV.

An attractive contribution to the interaction of nucleons may be described by a fourth order term in the chiral fields, introduced in ref. [12,13] :

$$\mathcal{L}_3 = \frac{\gamma}{8e^2}\left[Tr\left\{\partial_\mu U\, \partial^\mu U^\dagger\right\}\right]^2 \tag{2.4}$$

Alternatively, we can use the original Skyrme fourth order term (with the opposite sign) [13,14]

$$\mathcal{L}_4 = -\frac{\eta^2}{4} Tr\left\{\left[U^\dagger\partial_\mu U, U^\dagger\partial_\nu U\right]\cdot\left[U^\dagger\partial^\mu U, U^\dagger\partial^\nu U\right]\right\} \tag{2.5}$$

It is possible to model the influence of the vector meson by a sixth order term in the chiral fields in the Lagrangian [14,15],

$$\mathcal{L}_5 = \frac{\epsilon_6}{f_\pi^2} Tr\left\{\tilde{B}_\mu\tilde{B}^\mu\right\} \tag{2.6}$$

with the current

$$B^\mu = Tr\left\{\tilde{B}^\mu\right\}, \qquad \tilde{B}^\mu = \frac{\epsilon^{\mu\alpha\beta\gamma}}{24\,\pi^2} U^\dagger\partial_\alpha U\, U^\dagger\partial_\beta U\, U^\dagger\partial_\gamma U \tag{2.7}$$

Our reason for the introduction of this sixth order term is not so much a desire to include the vector meson into the calculation but instabilities in the chiral degrees of freedom (see section 4).

We have also introduced two other terms of sixth order in the meson fields, namely

$$\mathcal{L}_6 = -\frac{\delta_1}{8f_\pi^2}\left(Tr\left\{U^\dagger\partial_\mu U U^\dagger\partial^\mu U\right\}\right)^3 \tag{2.8}$$

and

$$\mathcal{L}_7 = \frac{\delta_2}{8f_\pi^2} Tr\left\{[U^\dagger\partial_\mu U, U^\dagger\partial_\nu U][U^\dagger\partial^\mu U, U^\dagger\partial^\nu U]\right\}\cdot Tr.\left\{U^\dagger\partial_\rho U U^\dagger\partial^\rho U\right\} \tag{2.9}$$

in our quest for a reasonable interaction energy between the solitons.

To justify the ansatz for the meson fields, we have to consider yet another term in the Lagrangian, introduced into the σ model by Gell-Mann and Levy [16]

$$\mathcal{L}_8 = \lambda(\sigma^2 + \pi^2 - f_\pi^2)^2 \tag{2.10}$$

Assuming $\lambda \gg 1$ we solve one of the two Lagrange equations for the chiral fields by the Hegdehog ansatz:

$$\sigma(\vec{r}) = f_\pi \cos\Theta(r)$$

$$\vec{\pi}(\vec{r}) = f_\pi \frac{\vec{r}}{r}\sin\Theta(r) \tag{2.11}$$

The remaining equation determines the chiral angle Θ . With the ansatz 2.11 we obtain for the sum of $\mathcal{L}_1, ..\mathcal{L}_8$

$$\begin{aligned}\mathcal{L} &= \bar{\Psi}\left[i\gamma_\mu\partial^\mu - g f_\pi(\cos\Theta + i\gamma_5\frac{\vec{\tau}\cdot\vec{r}}{r}\sin\Theta)\right]\Psi \\ &\quad -\frac{1}{2}f_\pi^2\left[\Theta'^2 + \frac{2\sin^2\Theta}{r^2}\right] + 8\eta^2\frac{\sin^2\Theta}{r^2}\left[\Theta'^2 + \frac{\sin^2\Theta}{2r^2}\right]\end{aligned}$$

$$+\frac{\gamma}{2e^2}\left[\Theta'^2+\frac{2\sin^2\Theta}{r^2}\right]^2-\frac{\epsilon_6}{8\pi^4 f_\pi^2}\Theta'^2\left(\frac{\sin\Theta}{r}\right)^4-\frac{\delta_1}{f_\pi^2}\left(\Theta'^2+\frac{2\sin^2\Theta}{r^2}\right)^3$$

$$-\frac{8\delta_2}{f_\pi^2}\frac{\sin^2\Theta}{r^2}\left(\Theta'^4+\frac{5}{2}\frac{\sin^2\Theta}{r^2}\Theta'^2+\frac{\sin^4\Theta}{r^4}\right) \tag{2.12}$$

Choosing the dimensionless parameters $\gamma, \eta, \epsilon_6, \delta_1$ and δ_2 appropriately we can test the various parts of the Lagrangian 2.12.

3. Field Equations

3.1 Dirac Hamiltonian

We treat the Dirac field in second quantization but omit all vacuum contributions. From the Lagrangian 2.12 we obtain an eigenvalue equation for the field operator Ψ with the Dirac-Hamiltonian:

$$H_D = -i\vec{\alpha}\cdot\vec{\nabla} + gf_\pi(\gamma_0\cos\Theta + i\gamma_0\gamma_5\frac{\vec{\tau}\cdot\vec{r}}{r}\sin\Theta) \tag{3.1}$$

We choose it's eigensolutions as basis states for the quarks. H_D commutes with the sum of angular momentum and isospin, the 'grand spin' $\vec{G}$, the parity operator $P = \gamma_0 P(\vec{r}\to-\vec{r})$ and does not act on the the color degree of freedom. Thus, the quark state can be labeled by G, the magnetic quantum number M of the grand spin, the parity π and the color quantum number. For the uniform background meson field $\Theta \equiv 0$ we recover from eq. 3.1 the free Dirac Hamiltonian for a particle with mass $m = gf_\pi$.

We first review the case that the parity equals $(-)^G$ (for the oppposite parity see the end of this subsection). Then, the following ansatz for the eigenstates of H_D [10] leads to a solution:

$$u_{c,G^\pi,M} = (gf_\pi)^{\frac{3}{2}}\begin{pmatrix} f_1(r)\,\mathcal{Y}_1^{G,M} + f_2(r)\,\mathcal{Y}_2^{G,M} \\ i\,g_1(r)\,\mathcal{Y}_3^{G,M} + ig_2(r)\,\mathcal{Y}_4^{G,M}\end{pmatrix} \mid c> e^{-iet} \tag{3.2}$$

$\mid c>$ denotes the color wave function. The intrinsic states $\mathcal{Y}_i^{G,M}$ depend on the polar angles θ, ϕ, the spin and isospin coordinates and read [10]

$$\begin{aligned}
\mathcal{Y}_1^{G,M} &= \mid 00> \; Y_{G,M}(\theta,\phi) \\
\mathcal{Y}_2^{G,M} &= \sum_{m=-1}^{1}(G\,M-m\,1\,m\mid G\,M) \quad \mid 1m> \; Y_{G,M-m}(\theta,\phi) \\
\mathcal{Y}_3^{G,M} &= \sum_{m=-1}^{1}(G+1\,M-m\,1\,m\mid G\,M) \quad \mid 1m> \; Y_{G+1,M-m}(\theta,\phi) \\
\mathcal{Y}_4^{G,M} &= \sum_{m=-1}^{1}(G-1\,M-m\,1\,m\mid G\,M) \quad \mid 1m> \; Y_{G-1,M-m}(\theta,\phi)
\end{aligned} \tag{3.3}$$

with

$$
\begin{aligned}
(\vec{s}+\vec{t})^2 \mid 00> &= 0 \\
(\vec{s}+\vec{t})^2 \mid 1m> &= 2 \mid 1m> \\
(\vec{s}+\vec{t}) \mid 1m> &= m \mid 1m>
\end{aligned}
\tag{3.4}
$$

For G = 0, the intrinsic states $\mathcal{Y}_2$ and $\mathcal{Y}_4$ disappear and we recover the well known ansatz [10] :

$$
u_{c,0+} = \frac{(g f_\pi)^{\frac{3}{2}}}{(4\pi)^{\frac{1}{2}}} \begin{pmatrix} f_1(r) \\ -i\,\vec{\sigma}\cdot\vec{e}_r\, g_1(r) \end{pmatrix} \mid 00> \mid c> e^{-i\epsilon t}
\tag{3.5}
$$

The radial functions f_i, g_i have to be calculated by solving the eigenvalue equation

$$
H_D\, u_{c,G^\pi,M} = \epsilon_{G^\pi}\, u_{c,G^\pi,M}
\tag{3.6}
$$

or, in more detail

$$
\begin{aligned}
\left(\frac{d}{dr} - \frac{G}{r} - \frac{m\,\sin\Theta}{2G+1}\right) F_1 \quad - (\epsilon + m\,\cos\Theta) g_1 &= 2\,\frac{\sqrt{G(G+1)}}{2G+1}\, m\,\sin\Theta\, F_2 \\
\left(\frac{d}{dr} + \frac{G+1}{r} + \frac{m\,\sin\Theta}{2G+1}\right) F_2 + (\epsilon + m\,\cos\Theta) g_2 &= 2\,\frac{\sqrt{G(G+1)}}{2G+1}\, m\,\sin\Theta\, F_1 \\
\left(\frac{d}{dr} + \frac{G+2}{r} + \frac{m\,\sin\Theta}{2G+1}\right) g_1 + (\epsilon - m\,\cos\Theta) F_1 &= 2\,\frac{\sqrt{G(G+1)}}{2G+1}\, m\,\sin\Theta\, g_2 \\
\left(\frac{d}{dr} - \frac{G-1}{r} - \frac{m\,\sin\Theta}{2G+1}\right) g_2 - (\epsilon - m\,\cos\Theta) F_2 &= 2\,\frac{\sqrt{G(G+1)}}{2G+1}\, m\,\sin\Theta\, g_1
\end{aligned}
\tag{3.7}
$$

Here, we have introduced linear combinations of f_1 and f_2, namely

$$
\begin{aligned}
F_{1,G^\pi} &= \frac{1}{\sqrt{2G+1}}\,(\sqrt{G+1}\, f_{1,G^\pi} + \sqrt{G}\, f_{2,G^\pi}) \\
F_{2,G^\pi} &= \frac{1}{\sqrt{2G+1}}\,(\sqrt{G}\, f_{1,G^\pi} - \sqrt{G+1}\, f_{2,G^\pi})
\end{aligned}
\tag{3.8}
$$

The equations 3.7 do not depend on the magnetic quantum number M or the color. Therefore, the functions F_i, g_i and the eigenvalue ϵ can be classified by the grand spin and the parity alone.

The ansatz for states with the parity $\pi = (-1)^{G+1}$ is obtained by multiplying $u_{c,G^\pi,M}$ (eq. 3.2) with γ_5. In the eqs. 3.7 this leads to a sign change of m and nothing else.

3.2 The Quark State

According to ancient literature [17] we have to put three quarks into the eigenstates of H_D to form a nucleon. To be consistent with the Hegdehog ansatz 2.11 we have to choose these states in a manner that $\underline{< S \mid \bar{\Psi}\Psi \mid S >}$ does not depend on the polar angles ($\mid S >$ is the 3-quark state). Additionally, $\underline{< S \mid \bar{\Psi}\gamma_5\vec{\tau}\Psi \mid S >}$ has to have the form $\vec{r} \cdot f(r)$. With the bar below the matrix element we denote here that a summation over spin, isospin and matter-antimatter degrees of freedom is carried out but no $\vec{r}$ integration.

The choice for $\mid S >$ in the literature [8,9,10,18] is:

$$\mid S1 >= a^{\dagger}_{G^{\pi}=0^+,r}\, a^{\dagger}_{G^{\pi}=0^+,g}\, a^{\dagger}_{G^{\pi}=0^+,b} \mid vac > \tag{3.9}$$

The operators $a^{\dagger}$ obey the usual anticommutator rules for Fermi operators and (r,g,b) are the color indizes. $\mid S1 >$ fulfills the conditions mentioned above (see appendix A).

However, we find alltogether twenty ways to arrange the quarks which are consistent with the Hegdehog approach and color neutrality. For instance, one, two or all three of the quarks may occupy the 0^- instead of the 0^+ state without violating the spherical symmetry of the Hedgehog ansatz. It is also possible to put one quark in the 1^+ or 1^- state, if we make use of the fact that the number of magnetic substates is equal to the number of colors:

$$\mid S2 >= \frac{1}{\sqrt{3}}\Big(a^{\dagger}_{1+,M=1,r}\, a^{\dagger}_{0+,g}\, a^{\dagger}_{0+,b} + a^{\dagger}_{1+,M=0,g}\, a^{\dagger}_{0+,b}\, a^{\dagger}_{0+,r} + a^{\dagger}_{1+,M=-1,b}\, a^{\dagger}_{0+,r}\, a^{\dagger}_{0+,g}\Big) \mid vac > \tag{3.10}$$

Similiar combinations including e.g. a 0^+ and two 1^+ states or a 0^-, 1^+ and 1^- state can be constructed. If we'd like to have all three quarks in a G=1 state, simpler terms like

$$\mid S3 >= a^{\dagger}_{1-,M=1,r}\, a^{\dagger}_{1-,M=0,g}\, a^{\dagger}_{1-,M=-1,b} \mid vac > \tag{3.11}$$

suffice. We have not succeeded in finding quark combinations involving grand spins bigger than one, which are compatible with Hegdehog-shaped meson fields.

The structure of the soliton ground state is not clear from the onset. We have to determine which of the quark levels involved is filled, raised from the Dirac sea by the meson field, and which is vacant. This is done by calculating the quark levels for decreasing meson field strength, i.e. decreasing coupling constants, and observing whether the level disappears into the Dirac sea or into the region of unbound quarks. The meson field used is either kept constant, determined for a fixed gf_{π} with $\mid S1 >$ or $\mid S2 >$, or it is calculated selfconsistent with the quark state. We have applied this procedure only for the second Lagrangian tested in section 4 and assume that the results concerning vacancy of quark levels are the same for the other Lagrangians considered. To give some results prematurely, it

turns out that the quark configuration $| S1 >$ appears as the soliton ground state and $| S2 >$ as the first excited state for a soliton.

We'd like to stress here that our Lagrangian leads to color neutrality for the soliton ground state without introducing explicit color dependent terms in the Lagrangian: since isospin and spin of the quarks are fixed in the 0^+ state, it admits only three quarks which have to have different colors according to the Pauli principle. Excited states like $| S3 >$, however, could be constructed colored at the same energy as the corresponding white states.

Regarding angular momentum $\vec{J}$ and isospin $\vec{T}$ of our soliton, we note that the chiral fields in the Hegdehog configuration 2.11 do not contribute to these quantities. They are carried exclusively by the quarks. In the state $| S1 >$, which is like $| S2 >$ not an eigenstate of $\vec{J}$ or $\vec{T}$ we have

$$< S1 \mid T^2 \mid S1 > = < S1 \mid (\vec{L} + \vec{S})^2 \mid S1 > = \frac{9}{4} \tag{3.12}$$

and for $| S2 >$

$$< S2 \mid T^2 \mid S2 > = \frac{9}{4}$$

$$< S2 \mid (\vec{L} + \vec{S})^2 \mid S2 > =$$

$$\frac{9}{4} + (g f_\pi)^3 \int_0^\infty r^2 dr \, (3 \, F^2_{1,G^\pi=1^+} \; + \; 6 \, g^2_{1,G^\pi=1^+}) \tag{3.13}$$

3.3 The Meson Field

The Euler-Lagrange equation for the the chiral meson field, expressed in terms of the angle Θ, reads:

$$\frac{g^4 f_\pi^4 r^4}{4\pi}[3(g_1^2 - f_1^2)\sin\Theta - 6 f_1 g_1 \cos\Theta] \; =$$

$$(f_\pi r)^2[(r^2\Theta')' - \sin(2\Theta)]$$

$$- 8\eta^2[2\Theta'' r^2 \sin^2\Theta + \Theta'^2 r^2 \sin(2\Theta) - \sin^2\Theta \sin(2\Theta)]$$

$$- \frac{2\gamma}{e^2}[3\Theta''\Theta'^2 r^4 + 2\Theta'^3 r^3 + 2\Theta'' r^2 \sin^2\Theta + \Theta'^2 r^2 \sin(2\Theta) - 2\sin^2\Theta \sin(2\Theta)]$$

$$+ \frac{\epsilon_6 \sin^2\Theta}{4\pi^4 f_\pi^2 r^2}[\Theta'' r^2 \sin^2\Theta - 2\Theta' r \sin^2\Theta + \Theta'^2 r^2 \sin(2\Theta)]$$

$$+ \frac{6\delta_1}{f_\pi^2 r^2}[\Theta'' r^2 (5\Theta'^4 r^4 + 12\Theta'^2 r^2 \sin^2\Theta + 4\sin^4\Theta) \; + \; 2\Theta'^5 r^5$$

$$+ 3\Theta'^4 r^4 \sin(2\Theta) + 4\Theta'^2 r^2 \sin^2\Theta \sin(2\Theta) - 8\Theta' r \sin^4\Theta - 4\sin^4\Theta \sin(2\Theta)]$$

$$+ \frac{8\delta_2}{f_\pi^2 r^2}[\Theta'' r^2 \sin^2\Theta (12\Theta'^2 r^2 + 5\sin^2\Theta) \; + \; 3\Theta'^4 r^4 \sin(2\Theta)$$

$$+5\Theta'^2 r^2 \sin^2\Theta \sin(2\Theta) - 10\,\Theta' r \sin^4\Theta - 3\sin^4\Theta \sin(2\Theta)] \tag{3.14}$$

in case the quarks occupy the state $\mid S1 >$. For the solution of the differential equations for the soliton, we iterate between eqs. 3.14 and 3.6 .

The mass of the free soliton is calculated as the volume integral of the Hamilton density:

$$\begin{aligned}
\int \mathcal{H}\, d^3r &= M \\
&= \sum_{occ.} \epsilon_i + 2\pi \int_0^\infty dr \Bigg[f_\pi^2 [\Theta'^2 r^2 + 2\sin^2\Theta] - \frac{\gamma}{e^2 r^2}[\Theta'^2 r^2 + 2\sin^2\Theta]^2 \\
&\quad - 16\eta^2 \frac{\sin^2\Theta}{r^2}[\Theta'^2 r^2 + \frac{1}{2}\sin^2\Theta] \\
&\quad + \frac{\epsilon_6}{4\pi^4 f_\pi^2}\Theta'^2 r^2 \left(\frac{\sin\Theta}{r}\right)^4 + \frac{2\delta_1}{f_\pi^2 r^4}[\Theta'^2 r^2 + 2\sin^2\Theta]^3 \\
&\quad + \frac{16\delta_2}{f_\pi^2 r^4}[\Theta'^4 r^4 \sin^2\Theta + \frac{5}{2}\Theta'^2 r^2 \sin^4\Theta + \sin^6\Theta] \Bigg]
\end{aligned} \tag{3.15}$$

3.4 Nuclear Matter

As in ref. [10] we describe nuclear matter by placing the solitons on a cubic lattice. We use the Wigner-Seitz approximation, which replaces the cubic problem by a spherically symmetric one [10,19], that is, each soliton sits in a spherical cell of radius R with specific boundary conditions on the surface of the sphere. The distance to the next neighbors is $2R$. This is a much simpler approach than a three dimensional calculation with cubic boundaries as performed in ref. [20] for the Skyrmion or in ref. [11] for a hybrid soliton. Nonetheless, we should get reliable results at least for the bottom of the ground state band according to ref. [19].

The treatment of excited quark states is different in the case of the free soliton from the case of the nucleonic crystal. While in the former case each quark configuration has to be calculated selfconsistent with the meson field, the average meson field in the crystal is not affected by an excitation of a sea- or valence quark. Therefore, the meson field for the crystal is calculated with the ground state configuration $\mid S1 >$ and then kept fixed for the determination of the other quark levels via eq. 3.6.

The levels in the crystal are, of course, split apart into bands by the interaction between the solitons. By the procedure mentioned above we obtain either the top of the band (for levels from the Dirac sea) or the bottom, since we assumed that the crystal momentum $\vec{k}$ [19,21] of each state is equal to zero. But for the calculation of the soliton-soliton potential we need the quark energies in the whole 0^+- valence band. Therefore we have to solve, with Bloch's ansatz $e^{i\vec{k}\cdot\vec{r}} u_{\vec{k}}$ for the wave function with a crystal momentum $\vec{k}$,

$$\left(H_D + \vec{\alpha}\cdot\vec{k}\right) u_{\vec{k},c,0^+} = \epsilon_k u_{\vec{k},c,0^+} \qquad with \quad u_{\vec{k}=\vec{0},c,0^+} = u_{c,0^+} \tag{3.16}$$

for all $\vec{k}$-vectors within the first Brillioun zone [19,21]. We do this by expanding $u_{\vec{k},c,0+}$ into the eigenfunctions of H_D:

$$u_{\vec{k},c,0+} = \sum_{G,\pi,M} A_{\vec{k},G,\pi,M} \; u_{c,G^\pi,M} \tag{3.17}$$

Projecting with the eigenfunctions of H_D in eq. 3.16 then leads to a matrix eigenvalue problem. Since we use the Wigner-Seitz approximation, the value of ϵ_k does not depend on the direction of $\vec{k}$ and we can choose it parallel to $\vec{e}_z$. The boundaries of the band in $\vec{k}$ space are given by the distance $2R$ between two solitons: [10,19,21]

$$-\frac{\pi}{2R} \leq k_x, k_y, k_z \leq \frac{\pi}{2R} = k_B \tag{3.18}$$

The number of states $d\,n(k)/d\,k$ for each value of $\mid \vec{k} \mid$ in the band can be easily calculated and is depicted in fig. 1. The matrix elements of α_z, needed for the diagonalization of 3.16, are given in appendix B.

It turns out that at small cell separations the valence band and the first excited one, a 1^+ band, intersect. In this case the valence band is no longer fully occupied and we have to determine the fermi energy ϵ_f, up to which both bands are filled. The procedure described above for the calculation of the valence band was therefore also applied to the 1^+ band (see appendix B), keeping in mind that the 1^+ state can be occupied by three times the number of quarks which fit into the valence state, since it has three magnetic substates. For the $M = \pm 1$ substates, spherical symmetry is lost even within the Wigner-Seitz approximation. To restore the spherical approach, we assume that the function $d\,\epsilon_{\vec{k},1+}/d\,n$, calculated with the $M = 0$ state for $\vec{k}$ parallel $\vec{e_z}$, is a reasonable representation of the actual population of the band.

To calculate the mass of the soliton within the crystal we now have to replace the quark contribution in eq. 3.15 with

$$\sum_{occ.} \epsilon_i \quad \longrightarrow \quad \sum_{occ.} \int_0^{k_F} \epsilon_{i,k} \frac{d\,n(k)}{d\,k} dk \; =: \; 3\bar{\epsilon} \tag{3.19}$$

In principle, we also would have to average the quark contributions in eq. 3.14 over the valence band and, eventually, the 1^+ band. An iteration between the determination of the meson field for a fixed quark contribution, and the calculation of the quark wave functions $u_{\vec{k},c,0+}$ for a fixed meson field would have to take place. For simplicity, we have assumed that the quark wave functions in the $\vec{k} = 0$ state of the valence band represent a reasonable approximation to the correct quark distribution for the calculation of the chiral angle.

3.5 Boundary Conditions for the Meson Field and the Quark Wave Functions

As already derived in 1961 the values of Θ at the origin and at infinity must differ by an integer multiple, B, of π, which was identified with the baryon number by

Skyrme [4]. In addition, there should be no pion field outside the soliton. In an earlier paper [10] the boundary conditions for the chiral angle were chosen to be $\Theta(0) = 0$, $\Theta(\infty) = \pi$ (B = 1), which leads to a $G^\pi = 0^-$ valence state for the quarks. In order to obtain a more pleasing 0^+ valence state, we have switched here to the conditions:

$$\Theta(0) = -\pi; \;\; \Theta(\infty) = 0 \tag{3.20}$$

In the crystal we have to impose that $\sin(\Theta)$ vanishes at the cell boundary, e.g. $\Theta(R) = 0$, otherwise the pion field would exhibit a discontinuity. The value at the origin remains at $-\pi$, so that there be a unit topological charge in each cell. The choice $\Theta(0) = \pi$, $\Theta(\infty) = 0$, which is also common [8,13], corresponds to a sign change in m, the eigenvalue ϵ, and the conserved topological quantum number B of the Skyrme model[10], i.e. a transition from a soliton to an antisoliton.

The behaviour of the quark wave functions at the origin for grand spin G > 0 and parity $(-)^G$ can be derived from eq. 3.7 to be

$$\begin{aligned}
F_1(r) &= r^G \\
F_2(r) &= \alpha r^G \\
g_1(r) &= -\frac{r^{G+1}}{2G+3}\left(m+\epsilon+\frac{\alpha a}{\epsilon - m}\right) \\
g_2(r) &= \alpha r^{G-1}\,\frac{2G+1}{m-\epsilon}
\end{aligned} \tag{3.21}$$

where a is given by

$$a = 2\sqrt{G(G+1)}\,m\,\frac{d\Theta}{dr}\,|_{r=0} \tag{3.22}$$

and α is a parameter to be determined by adjusting it to the boundary conditions at the outside.

For the free soliton, we find at infinity with the parameter β :

$$\begin{aligned}
F_1(r\to\infty) &= \exp(-\sqrt{m^2-\epsilon^2}\,r) \\
F_2(r\to\infty) &= \beta\exp(-\sqrt{m^2-\epsilon^2}\,r) \\
g_1(r\to\infty) &= -\frac{\sqrt{m^2-\epsilon^2}}{m+\epsilon}\cdot F_1 \\
g_2(r\to\infty) &= \frac{\sqrt{m^2-\epsilon^2}}{m+\epsilon}\cdot F_2
\end{aligned} \tag{3.23}$$

and for the crystal, we deduce from the form of the wave function 3.2 the following conditions for the radial functions:

$$\begin{aligned}
g_1(R) &= 0 = g_2(R)\ , && G\ \textit{even} \\
F_1(R) &= 0 = F_2(R)\ , && G\ \textit{odd}
\end{aligned} \tag{3.24}$$

For G = 0 F_2 and g_2, or α and β, vanish. If the parity is $(-)^{G+1}$, the sign of m changes in the above equations.

The integration of eq. 3.7 is started from infinity for the free soliton; we use the parameter β and the eigenvalue ϵ to obtain $g_1(0) = 0, F_2(0) = 0$ at the origin. The other boundary conditions in eq. 3.21 are then automatically fulfilled. We start from the origin when calculating the quark wave functions in the Wigner-Seitz cell and use the parameter α and the eigenvalue ϵ to fulfill the two conditions 3.24 at the cell boundary.

4. Search for an appropriate Lagrangian

Throughout this section we assume that the state $| S1 >$ is the correct ground state for the quarks. We test the various Lagrangians introduced in section 2, looking for a reasonable behaviour of the interaction energy between the solitons in nuclear matter, i.e. a minimum around ground state nuclear matter density and a repulsive core for higher densities.

We start by showing the dependence of the soliton mass M, eqs. 3.15 and 3.19, on the cell size R for the hybrid soliton used in in ref. [10] (Fig. 2). The Lagrangian is $\mathcal{L}_1 + \mathcal{L}_2$ and we have no free parameter. Besides the results of the full calculation (solid line) we also present the meson contributions to the soliton mass (dashed line), i.e. the contributions from the integral in eq. 3.15. The dotted line shows the results of the intermediate step before calculating the valence band; for this curve all quarks are assumed to be in the $\vec{k} = 0$ state of the band. The average interaction potential between the solitons is obtained by subtracting the asymptotic mass, 940 MeV, from the soliton mass.

Fig. 2 reveals that there is no hint of an attractive part in the soliton-soliton interaction for this Lagrangian. Nuclear ground state density corresponds to a cell separation of R $\sim$ 0.94 fm and at this point the effects of the finite quark band width alone (the difference between the solid and the dotted line) add more than 300 MeV to the soliton mass, bringing the total to roughly 1400 MeV in each cell. In figure 3 we focus on the behaviour of the quark bands for this Lagrangian; we show width and location (in energy) of the valence band and the first excited band against the cell radius. Observe that the average quark energy is roughly in the center of the valence band for R = 1.5 fm, but almost at the upper end for smaller cell separations. This happens despite the intersection of the 0^+ and the 1^+ band at R = 0.8fm, which should open up a vast number of low lying states for the quarks. The net effect of this behaviour of the quark energy is an increase of 400 MeV in $\bar{\epsilon}$ (eq. 3.19) between R = 4 fm and 0.4 fm or an 1200 MeV increase in the soliton mass.

As a side remark, the soliton mass also behaves strangely for large R, it decreases by 14 MeV from $R = 3$ fm to 4 fm, (which corresponds to a change in ρ from $\rho_0/17$ to $\rho_0/40$), where no visible change in the energy should occur. This seems to be a common feature of Skyrmion like models [20]; apparently it is due to the $1/r^2$ fall-off (instead of exponential) of the chiral angle towards zero at the cell border.

In view of the above result we wanted to change the Lagrangian of the hybrid soliton. As a first try we included a fourth order term in the chiral fields into the

Lagrangian with a sign that guaranteed an attractive contribution to the potential. In addition, we introduced a stabilizing sixth order term in the meson field, $\mathcal{L}_5$, which is supposed to model the influence of the vector-meson [14,15]. Without this term, the soliton solution would be instable [22]. For the fourth order term we could choose between the newly proposed $\mathcal{L}_3$ [12] and the old Skyrme term $\mathcal{L}_4$ [4,13,14]. We find that $\mathcal{L}_4$ always leads to better results than $\mathcal{L}_3$, i.e. more attraction at ground state density, for the Lagrangians tested in this section. Therefore we display only results where $\mathcal{L}_4$ was used. Here, we had three parameters, the coupling constant g, the strength of the fourth order term, γ/e^2 or η, and of the sixth order term, ϵ_6. As in an earlier paper [10] the soliton mass is fitted to 940 MeV at R = 4 fm and we are left with two free parameters. These were adjusted in order to get a deep minimum in the dependence of the soliton mass on the cell radius. We had to realize, however, that it was impossible to obtain this minimum in the interaction energy, although we succeeded in getting it at approximately the right density in the intermediate step, where all quarks are assumed to have $\vec{k} = 0$ (see fig. 4). The kinetic energies of the quarks, due to the splitting up of the free soliton levels into the crystal band, add 400 MeV at $R = 1$ fm to the soliton mass and lead to the disappearance of the 50 MeV deep minimum which shows up in the dotted line (see fig. 5).

Why can't we just increase the value of either η or γ/e^2 and get the attraction we want? The reason, as was recognized already by several authors [12,13,22] is that above certain values of η or γ/e^2 no solution, i.e no minimum in the energy surface, exists for the chiral angle with the boundary conditions 3.20. The fourth order terms with the signs used here destabilize the soliton solution as can be seen from the expression for the soliton mass, eq. 3.15. Thus, there is an upper limit to the strength of the fourth order term.

Keeping this in mind we investigated if the dependence of our sixth order term on Θ' might be too weak to allow for a strong fourth order term. The destabilizing terms $\mathcal{L}_3$ and $\mathcal{L}_4$ include Θ' in fourth and second order, respectively, the stabilizing $\mathcal{L}_5$ only in second order. This means, our soliton is in principle unstable against the appearance of small wiggles in the function $\Theta(r)$ at least if we use $\mathcal{L}_3$.

That was the reason for introducing two other sixth order terms in the fields, $\mathcal{L}_6$ and $\mathcal{L}_7$, instead of the old one, making eq. 3.14 rather complicated looking. The dependence of these terms on Θ' is now of sixth and fourth order, respectively. To test each of them, we again can adjust two free parameters to find a minimum in the dependence of the soliton mass on the cell radius. The results of our quest are presented in figures 6a and 6b for the Lagrangians with $\mathcal{L}_6$ and $\mathcal{L}_7$, respectively. In both cases we obtain minima, approximately 200 MeV deep, in the intermediate step of the calculation (dotted line) and succeed in making a dent in the interaction potential. Nonetheless, the soliton mass is still 200 to 300 MeV too high at ground state nuclear matter density. Fig. 7 shows the quark bands for these cases: though the 1^+ band is occupied for R $\leq$ 1.5 fm, the average quark energy is about 100 MeV higher than the energy for $\vec{k} = 0$ at $R = 1$ fm and shows the same trends as before, i.e. a movement towards the upper end of the band for small cell separations.

Why is it that the occupation of the 1^+ band does not change the upward trend

of the average quark energy? The answer is depicted in the figures 8 and 9 for the third Lagrangian considered. There we see that the percentage of states in the 1^+ band never exceeds 25% of the total down to R = 0.4 fm, even so the total number of states available in this band is three times higher than in the valence band. Fig. 9 shows the development of the band structure in our calculation in more detail: at R = 3 fm, we have the two bands well separated in energy with the average energy right in the middle of each band; at R = 1 fm the two bands overlap between ϵ = 305 and 345 MeV and the density of states is highest towards the end of the bands. At R = 0.5 fm we see this development taken to its extremes: the valence band starts at 115 MeV and goes up to 310, but the number of states below 290 MeV is only 12% of the total. In our calculation, the 1^+ band shows a similiar, if not so pronounced development.

We should point out here that we use the rather crude Wigner-Seitz approximation for the calculation of the quark levels in the crystal. A full three-dimensional calculation in a cubic cell might change the results shown in figures 8 and 9 significantly, as the W.S. approximation is known to be not reliable for the details of the band structure [19]. We wanted to show these figures nonetheless to give an explanation for the behaviour of the average quark energy in figs. 3, 5 and 7.

Are the enormous kinetic quark energies we compute a special feature of our model or something that will appear in every model of the quark substructure of the nucleon? Let us take a look at the simple case of a noninteracting gas of relativistic Fermi particles with mass m. For this problem the average energy is given by

$$\bar{\epsilon} = 0.75\frac{\epsilon_F^3}{k_F^2} - \frac{3m^2}{8k_F}\left(\frac{\epsilon_F}{k_F} + \frac{m^2}{k_F^2}\log\frac{k_F+\epsilon_F}{m}\right) \tag{4.1}$$

where k_F is the Fermi momentum and $\epsilon_F = \sqrt{k_F^2 + m^2}$. The kinetic part of this energy is depicted in figure 10a for three different masses.

The relation between k_F and the particle density ρ is:

$$k_F = \left(\frac{6\pi^2\rho}{f}\right)^{1/3} \tag{4.2}$$

The number of particles, which can occupy a special $\vec{k}$ state, was here denoted with f. In our case, f is equal to the number of colors, since there is no freedom in the spin- and isospin coordinates in the valence state. Using eq. 4.2 and the relation

$$\rho = \frac{f}{8R^3} \tag{4.3}$$

we find the connection between the cell radius R and the kinetic energy for a free Dirac gas, where the number of particles in each cell is equal to f (Fig. 10b). Applying this figure to our specific problem, we find that for a quark mass of 400 MeV we will gain 3 times 100 MeV kinetic quark energy, if the quarks are compressed from a dilute gas to nuclear matter density (R = 0.94 fm). Up to this density, our average quark energies in figs. 3, 5 and 7 follow approximately the curve in fig.

10b for $m = 400$ MeV. For higher densities our increase in kinetic energy is smaller than the one for the free Dirac gas. This is due to rapid changes in the meson configuration and the opening up of the 1^+ band, but up to ground state density we see the same amounts of kinetic energy as depicted in fig. 10b. We assume that similiar amounts of kinetic energy should appear in every model of the nucleon containing quarks, where only three quarks fit in the ground state orbital. If the spin and isospin dependence of the quark energies is dropped (as e.g. in ref. [11] where f was equal to 12) these energies can be scaled down by a factor of three at R = 1 fm and higher amounts at higher densities (see eqs. 4.1, 4.2 and fig. 10a).

At this point, it seems that higher order terms in the meson field of the Lagrangian will not lead to a reasonable interaction energy of the solitons. It might be possible that improvements in the hybrid soliton model described in sections 2 and 3 will bring about the desired results without giving up the chiral symmetrie. In our opinion, two major steps could be tried: introduction of a new term in the Lagrangian for the quarks, which allows to create nucleons with proper spin and isospin and therefore isospin symmetric nuclear matter; and the execution of a fully three-dimensional calculation for the nucleonic crystal, i.e. dropping the Wigner-Seitz approximation.

5. Conclusions

We have examined one aspect of the hybrid soliton model, namely the behaviour of the interaction energy it predicts for infinite nuclear matter. To this end we have assumed that nuclear matter condenses in the form of a simple cubic crystal with the hybrid solitons at the centers of the basic cells. To render the calculation tractable we have employed the Wigner-Seitz approximation, which replaces the cubic cells of the crystal by spherical ones. We allowed ourselves a considerable freedom in the choice of the Lagrangian for the hybrid soliton, testing two fourth order and three sixth order terms in the meson fields with free strength parameters. Despite this freedom, the compression of the quarks in the nucleonic crystal adds such an enormous amount of energy to the soliton mass that we were unable to produce a potential with an attractive part at ground state nuclear matter density. A more accurate, three dimensional treatment of the nucleonic crystal might resolve this problem, but this seems doubtful.

We would like to thank D. Vasak and U. Mosel for many helpful discussions.

Appendix

A. Matrix elements with the quark state

For the determination of the equation for the chiral angle, we want to evaluate the matrix elements

$$\underline{< S1 \mid \bar{\Psi}\Psi \mid S1 >}$$

and

$$\underline{< S1 \mid \bar{\Psi}\gamma^5\vec{\tau}\Psi \mid S1 >}$$

which appear in the Euler-Lagrange equations for the sigma and the pion field, respectively. Remember that no r-integration is carried out for those matrix elements (see section 3.2). Inserting the field operator Ψ, we have

$$\begin{aligned}
&\underline{< S1 \mid \bar{\Psi}\Psi \mid S1 >} \\
&\quad = \sum_{n,m} u_n^\dagger \gamma_0 u_m \; < vac \mid u_{b,0+} u_{g,0+} u_{r,0+} \; u_n^\dagger u_m \; u_{r,0+}^\dagger u_{g,0+}^\dagger u_{b,0+}^\dagger \mid vac > \\
&\quad = 3\, u_{r,0+}^\dagger \, \gamma_0 \, u_{r,0+} \; + \sum_{occ} u_{occ}^\dagger \gamma_0 u_{occ} \\
&\quad \simeq 3\, u_{r,0+}^\dagger \, \gamma_0 \, u_{r,0+} \\
&\quad = \frac{3}{4\pi} (g f_\pi)^3 \, (F_1^2 - g_1^2)
\end{aligned} \tag{6.1}$$

where {occ} denotes all states occupied in the vacuum and the functions F_1 and g_1 are defined in eq.s 3.2 and 3.8. For the isospin dependent term, we get:

$$\underline{< S1 \mid \bar{\Psi}\gamma^5\vec{\tau}\Psi \mid S1 >} = \frac{3i}{2\pi} (g f_\pi)^3 \frac{\vec{r}}{r} f_1 \, g_1 \tag{6.2}$$

We combine the sigma and the pion equation in two manners; first, we multiply the sigma-equation with $\cos\Theta$ and the pion-equation with $\sin\Theta$ and add the two equations; second, we multiply the opposite way and subtract. The first attempt produces an equation, which includes the λ term arising from $\mathcal{L}_8$. It is approximately solved by the Hegdehog ansatz, when λ is large. The second attempt leads to eq. 3.14.

B. Matrix elements of α_z

The α_z operator couples the 0^+ quark level only to states with the magnetic quantum number M equal zero and the parity π equal $(-)^G$. For these levels we have:

$$\begin{aligned}
&< 0^+ \mid \alpha_z \mid G, M = 0, \pi = (-)^G > \\
&\quad = i\, \delta_{G,1} \, (g f_\pi)^3 \int_0^\infty r^2 \, dr \, \left[g_{2,G^\pi} \, F_{1,0+} - \frac{g_{1,0+}}{3} (2\sqrt{2} F_{1,G^\pi} - F_{2,G^\pi}) \right]
\end{aligned} \tag{6.3}$$

and

$$\begin{aligned}
&< G, M = 0, \pi = (-)^G \mid \alpha_z \mid H, M' = 0, \pi = (-)^H > \\
&\quad = i (g f_\pi)^3 \Bigg[\delta_{G,H-1} \int_0^\infty r^2 \, dr \left\{ \frac{g_{2,H}}{2G+1} (F_{1,G} + 2\sqrt{G(G+1)} F_{2,G}) \right.
\end{aligned}$$

$$+\frac{g_{1,G}}{2G+3}(2\sqrt{(G+1)(G+2)}F_{1,H}-F_{2,H})\Big\}$$

$$-\delta_{G,H+1}\int_0^\infty r^2\,dr\,\Big\{\frac{g_{2,G}}{2G-1}(F_{1,H}+2\sqrt{G(G-1)}F_{2,H})$$

$$+\frac{g_{1,H}}{2G+1}(2\sqrt{G(G+1)}F_{1,G}-F_{2,G})\Big\}\Big] \tag{6.4}$$

That is, α_z causes a coupling between the 0^+ and the 1^-, the 1^- and the 2^+, the 2^+ and the 3^- state, etc. .

Figure captions

*Fig.*1:

The density of states in the valence band versus the absolute value of the wave vector. Three different analytic expressions are needed for the calculation of this figure: two simple parabolic ones between 0 and k_B and between k_B and $\sqrt{2}k_B$ and a complicated expression for the rest up to $\sqrt{3}k_B$. The total number of states is normalized to 1.

*Fig.*2:

Soliton mass versus the cell radius in the crystal. The dashed line shows the contributions of the meson field and the solid line the results of the full calculation. The dotted line is the result of an intermediate step; here we assume all quarks to have the energy of the 0^+ state with $\vec{k} = \vec{0}$ at the bottom of the band. The Lagrangian used here is taken from ref. [10], it consists only of the kinetic energy of the chiral field, $\mathcal{L}_1$, and the quark Lagrangian $\mathcal{L}_2$. The coupling constant g is 5.89.

*Fig.*3:

The valence band in the nucleonic crystal for the Lagrangian described in the caption to fig.2. The shaded area between the 0^+ state with wave vector zero and the dashed line is occupied by quark levels with wave vectors between zero and $\sqrt{3}k_B$. The average quark energy is indicated by the full dots. The asymptotic quark mass, here 547.8 MeV, is given in the upper left. We also have included the first excited quark band, build on a 1^+ state. The intersection of the two bands at R = 0.8 fm marks the transition from a color isolator to a color conductor [10].

*Fig.*4:

Same as in fig. 2 for the Lagrangian $\mathcal{L} = \mathcal{L}_1 + \mathcal{L}_2 + \mathcal{L}_4 + \mathcal{L}_5$. The values of the parameters g, η^2 and ϵ_6 are: 4.47, 0.0055 and 1.24 .

*Fig.*5:

Same as in fig. 3 for the Lagrangian described in the caption to fig. 4.

*Fig.*6:

a.) Same as in fig. 2 for the Lagrangian $\mathcal{L} = \mathcal{L}_1 + \mathcal{L}_2 + \mathcal{L}_4 + \mathcal{L}_6$. The values of the parameters g, η^2 and δ_1 are: 3.65, 0.005 and 0.000015 .

b.) Same as in fig. 2 for the Lagrangian $\mathcal{L} = \mathcal{L}_1 + \mathcal{L}_2 + \mathcal{L}_4 + \mathcal{L}_7$. The values of the parameters g, η^2 and δ_2 are: 3.95, 0.0045 and 0.00001 .

*Fig.*7:

Same as fig. 3 for the Lagrangians described in figure 6. The asymptotic quark masses here are 339.45 MeV for fig. a) and 367.35 MeV fig. b) .

*Fig.*8:

Number of states in the 1^+ band versus cell radius for the Lagrangian used for fig. 6a.

*Fig.*9:

Density of states over the quark energy for the same Lagrangian used for figure 8. Three different cell separations are used: R is equal to 3 fm, 1 fm and 0.5 fm in figs. a), b) and c), respectively. The shaded area shows the occupied states, ϵ_f the Fermi energy and $\bar{\epsilon}$ the average energy. Two bands, the 0^+ and the 1^+ are involved. For R = 0.5 fm, the lower end of the bands had to be indicated, since the density

of states there was negligible. The number of states in the valence band has been normalized to one, the number in the 1^+ band to three.

*Fig.*10:

a.) Kinetic quark energy for free Dirac particles according to eq. 4.1 for three different masses versus the Fermi momentum.

b.) Same energy as in fig. a) versus the cell separation. The connection between the cell separation and the Fermi momentum has been made with the assumption, that each cell contains as many Dirac particles as fit in one state with fixed $\vec{k}$.

Bibliography

[1] G. t'Hooft, Nucl. Phys. B72 461(1974).

[2] E. Witten, Nucl. Phys. B160 57(1979).

[3] to give some recent publications on the subject :

K. Fujii, K.I. Sato, N. Toyota and A.P. Kobushkin, Phys. Rev. Lett. 58 651(1987);

T. Sato, Phys. Rev. D35 1888(1987);

J. Kunz and D. Masak, Phys. Lett. B184 253 (1987);

D.O. Rishka and E.M. Nyman, Phys. Lett. B183 7(1987);

M. P. Mattis, Phy. Rev. Lett. 56 1103(1986);

U. G. Meissner and I. Zahed, Phys. Rev. Lett. 56 1035(1986);

M.J. Bowick, D. Karabali, and L.C.R. Wijewardhana, Nucl. Phys. B271 417(1986);

E. Braten and L. Carson, Phys. Rev. Lett. 56 1897(1986) .

[4] T.H.R. Skyrme, Proc. Roy. Soc. A260 127(1986); Nucl. Phys. 31 556(1962).

[5] G.S. Adkins, C.R. Nappi and E. Witten, Nucl. Phys. B228 552(1983).

[6] D. Finkelstein and J. Rubinstein, Journal of Math. Phys. 9 1762(1968); E. Witten, Nucl. Phys. B223 422, 433(1983).

[7] M.D. Mattis and M. Karliner, Phys. Rev. D31 2833(1985).

[8] S. Kahana, G. Ripka and V. Soni, Nucl. Phys. A415 351(1984).

[9] M.C. Birse and M.K. Banerjee, Phys. Lett. 136B 284(1984).

[10] N.K. Glendenning and B. Banerjee, Phys. Rev. C34 1072(1986); B. Banerjee, N.K. Glendenning and V. Soni, Phys. Lett. B155 213(1985).

[11] J. Achtzehnter, W. Scheid and L. Wilets, Phys. Rev. D32 2414(1985).

[12] M. Lacombe, B. Loiseau, R. Vinh Mau and W.N. Cottingham, Phys. Lett. B161 31(1985); J.F. Donoghue, E. Golowich and B.R. Holstein, Phys. Rev. Lett. 53 747(1984) .

[13] D.E.L. Pottinger and E. Rathske, Phys. Rev. D33, 2448(1986).

[14] A. Jackson, A.D. Jackson, A.S. Goldhaber, and G.E. Brown, Phys. Lett. 154B 101(1985).

[15] D. Klabucar and G.E. Brown, Nucl. Phys. A454 589(1986).

[16] M. Gell-Mann and M. Levy, Nuovo Cimento 16 705(1960).

[17] M. Gell-Mann, Phys. Lett. 8 214(1964); G. Zweig, CERN Rep. TH 401, TH 412 (1964,1965) unpublished.

[18] S. Kahana and G. Ripka, Nucl. Phys. A429 462(1984).

[19] L. Pincherle, Electronic Energy Bands in Solids, London, Macdonald, 1971.

[20] I. Klebanov, Nucl. Phys. B262 133(1985).

[21] C. Kittel, Introduction to Solid State Physics, New York, Wiley, 1971.

[22] F.R. Klinkhamer, Zeitsch. f. Phys. C31 623(1986).

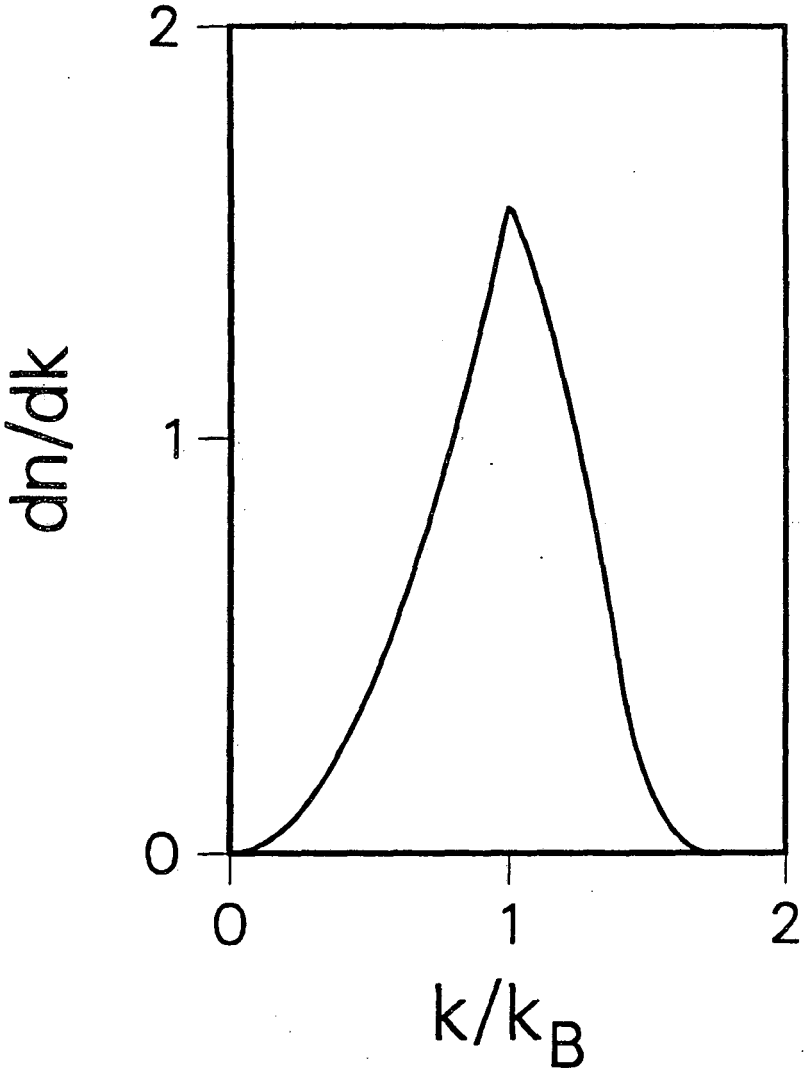

Figure 1

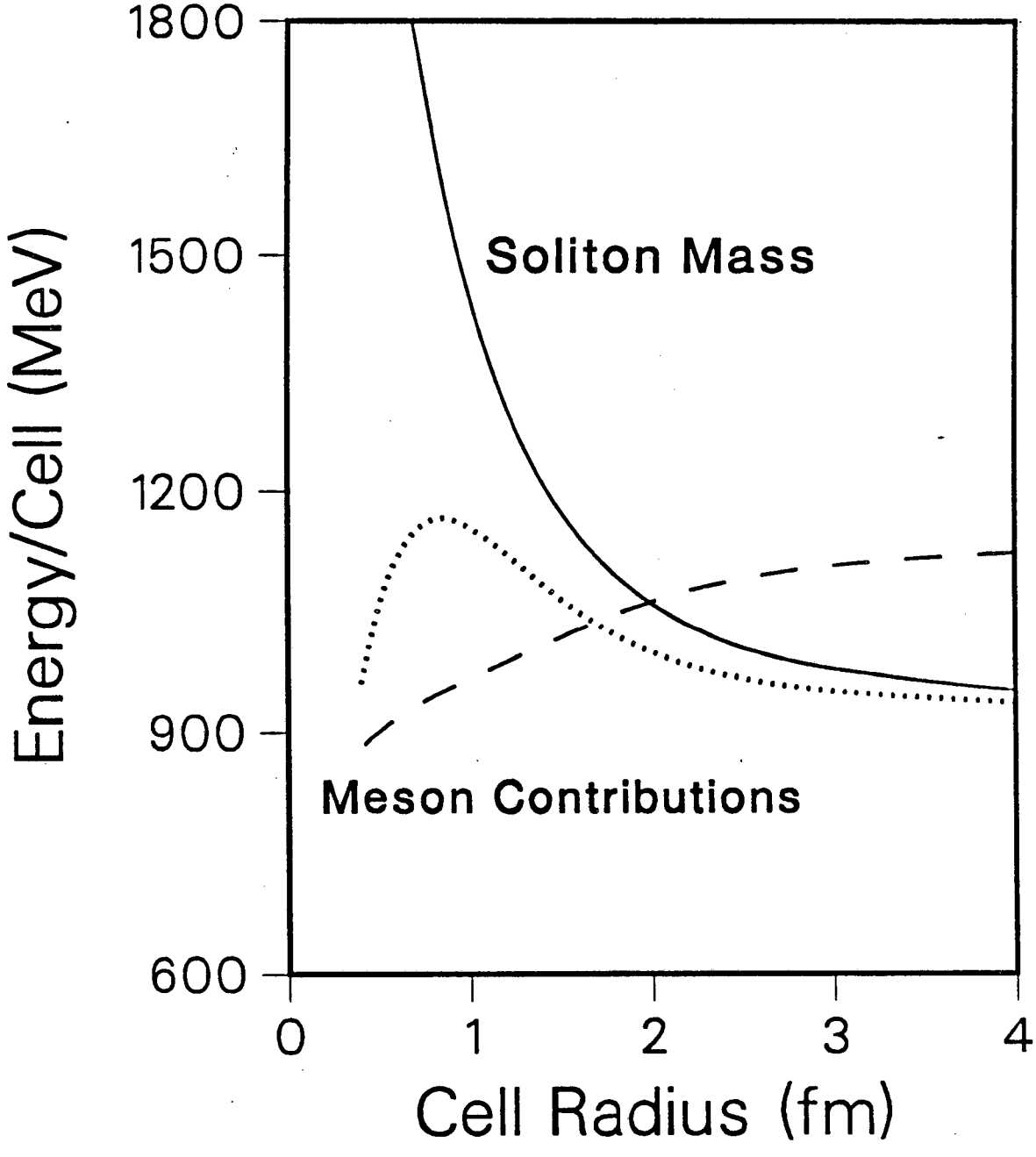
1800
1500
1200
900
600
Energy/Cell (MeV)
Soliton Mass
Meson Contributions
0
1
2
3
4
Cell Radius (fm)

Figure 2

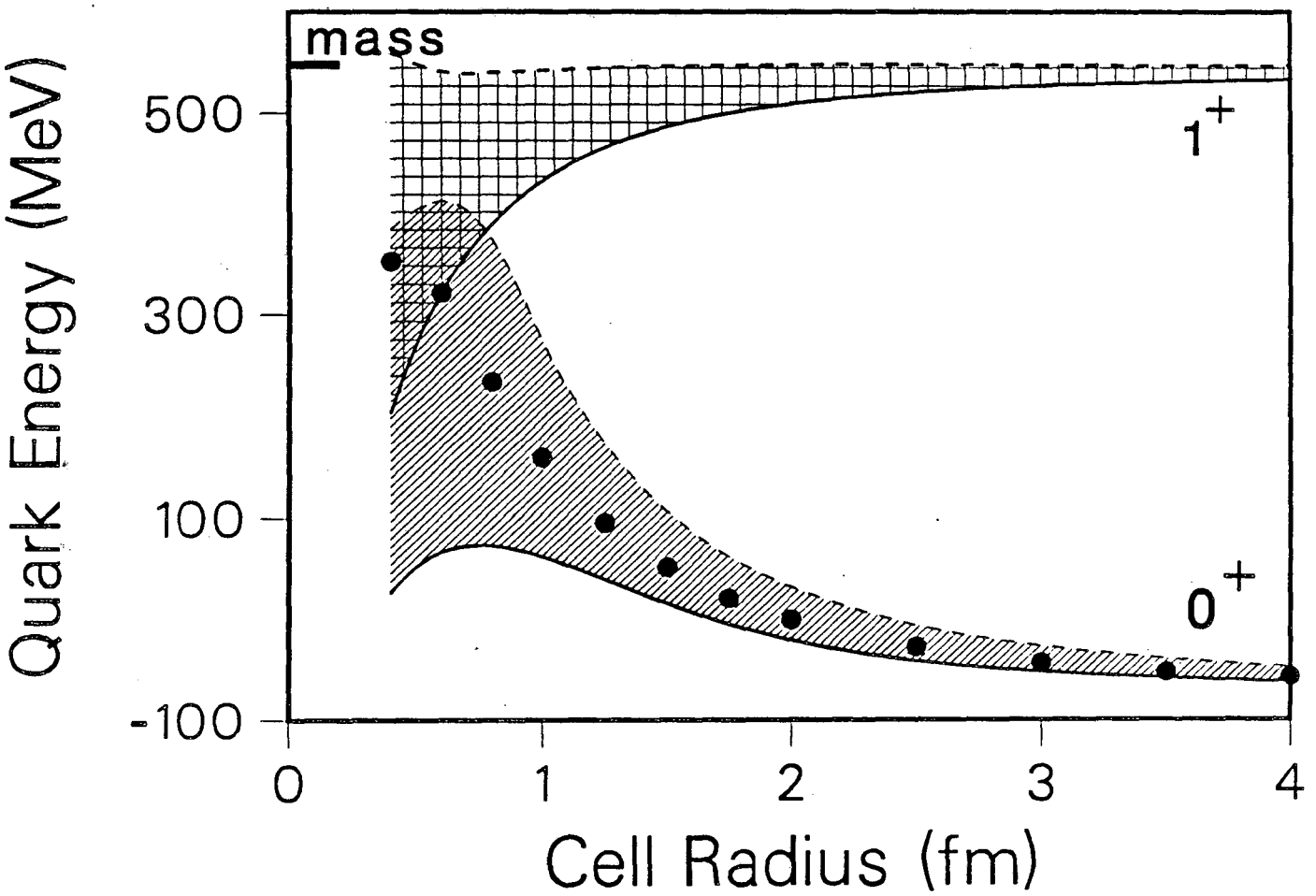

Figure 3

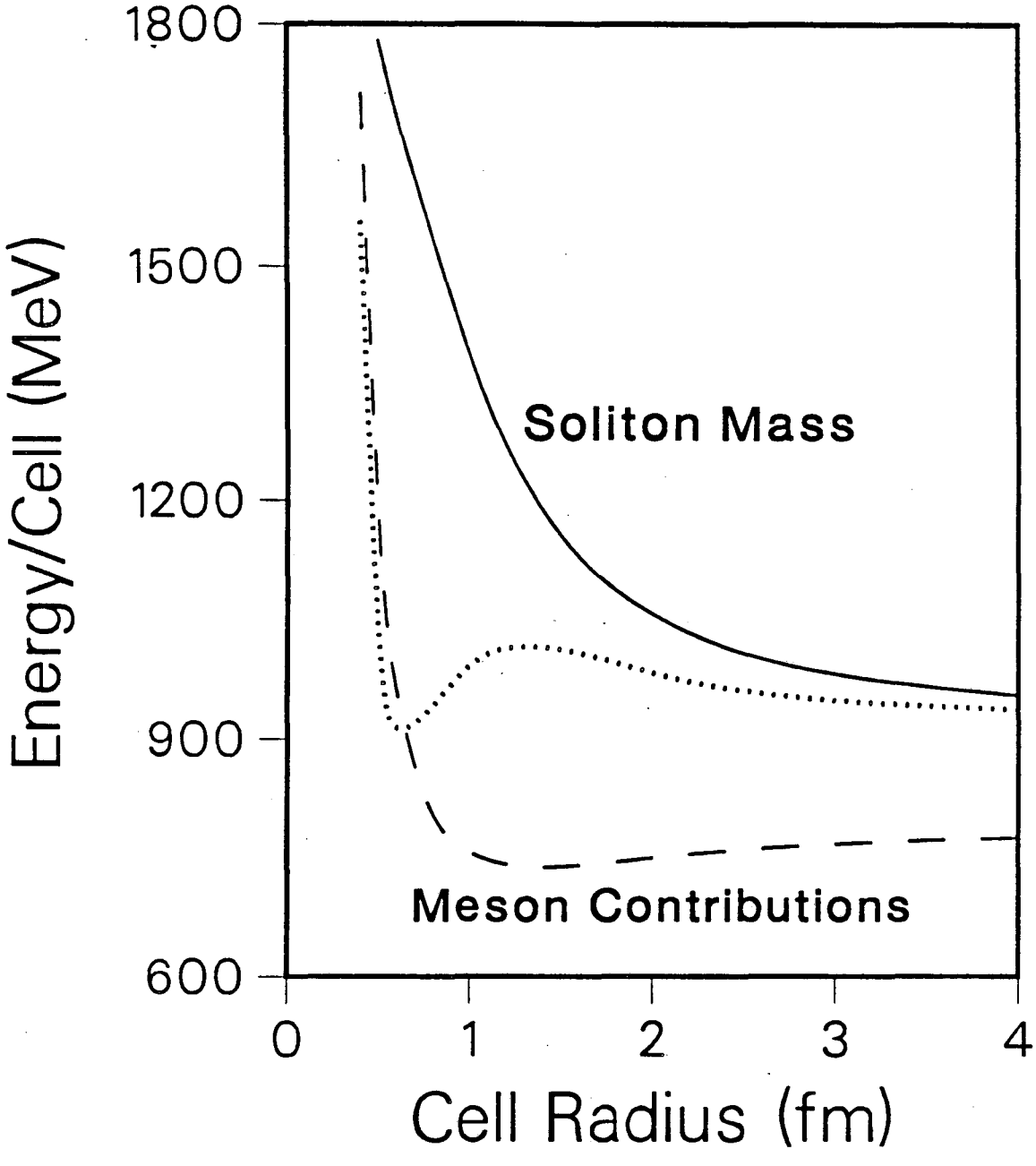
1800
1500
1200
900
600
Energy/Cell (MeV)
Soliton Mass
Meson Contributions
0
1
2
3
4
Cell Radius (fm)

Figure 4

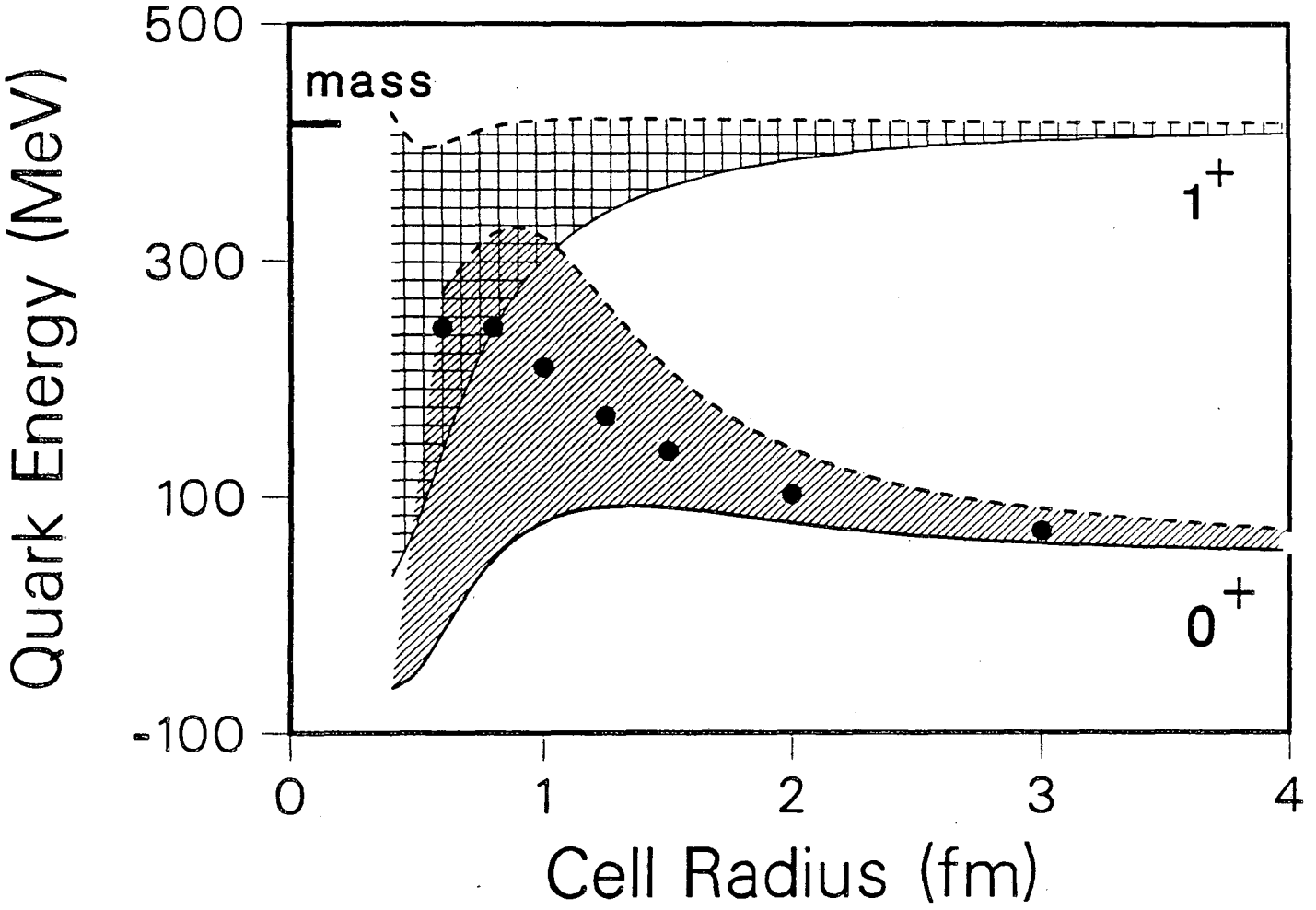

Figure 5

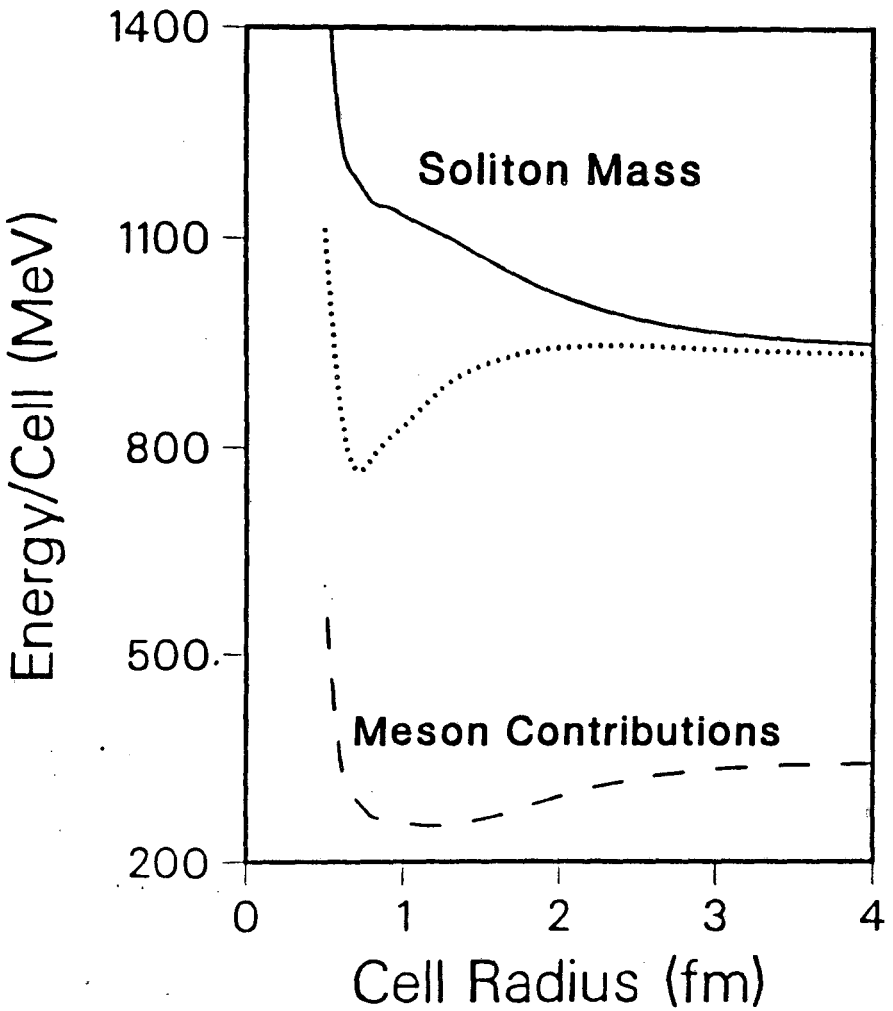

Figure 6a

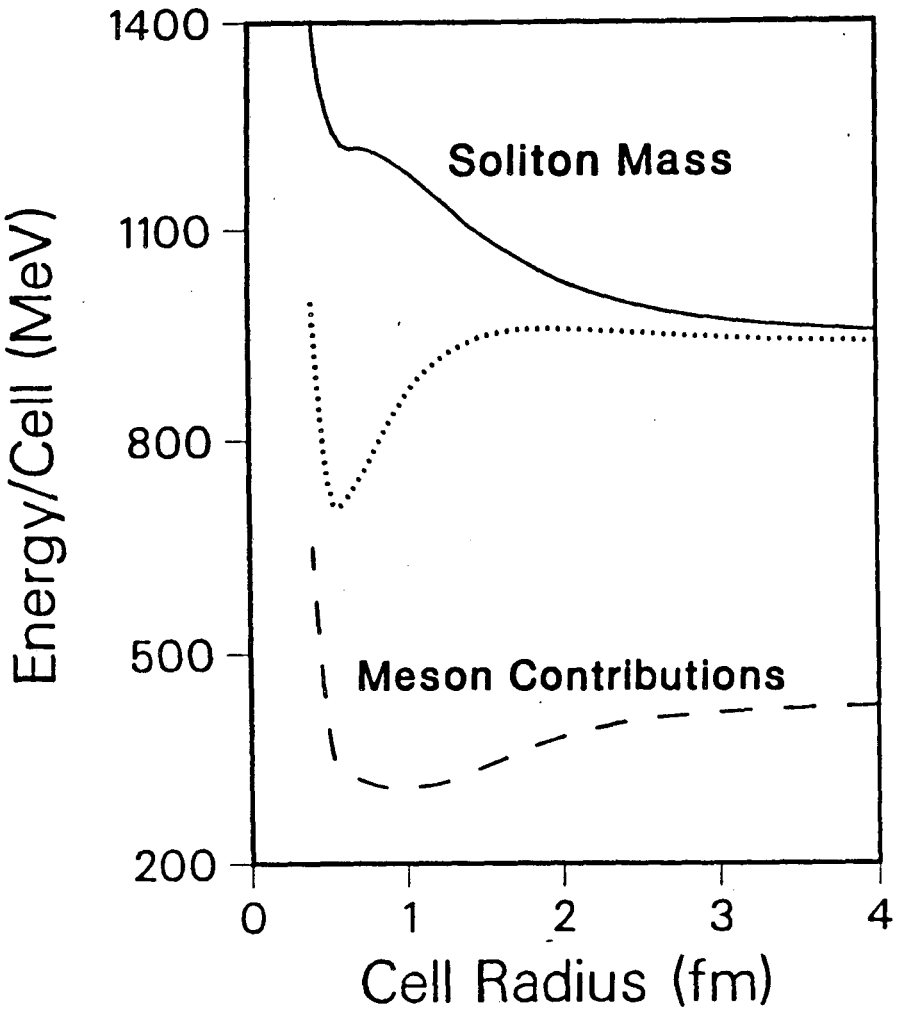

Figure 6b

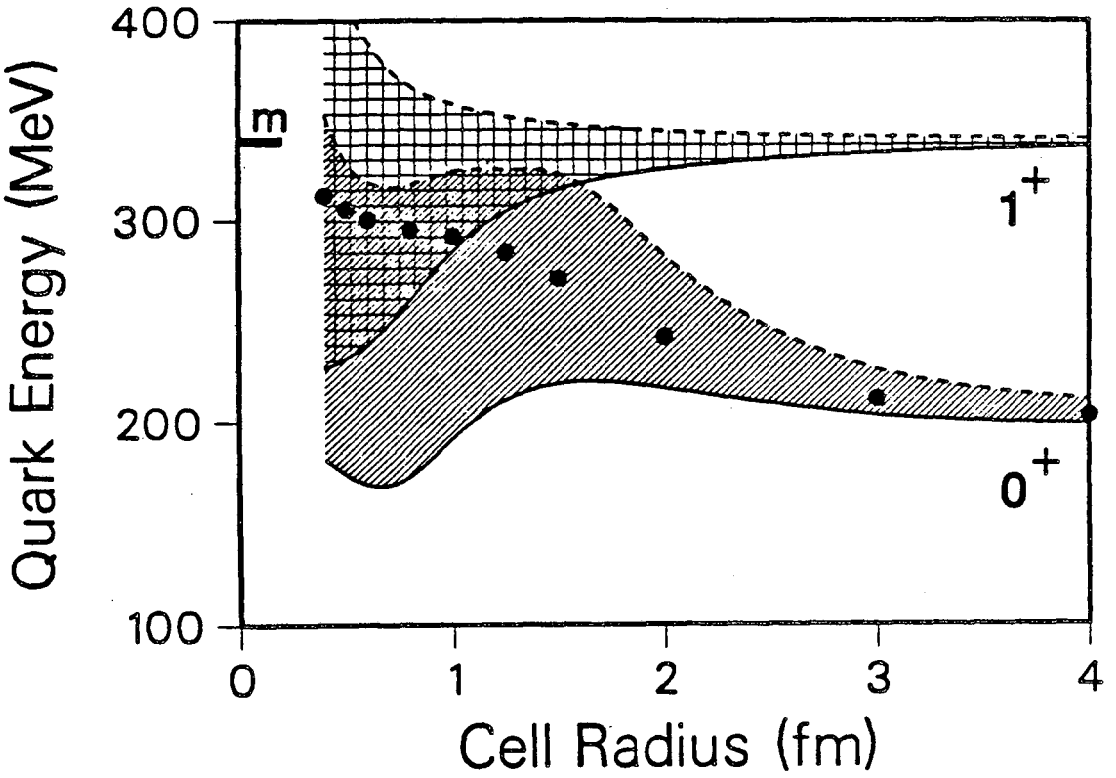

Figure 7a

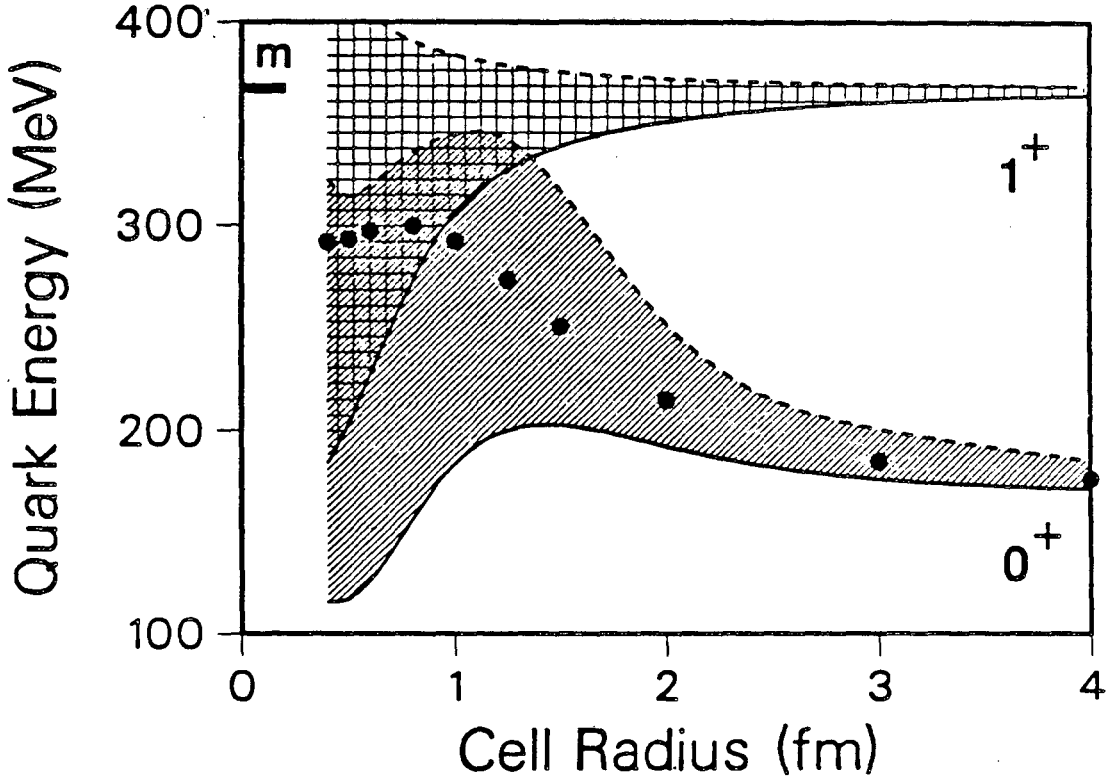

Figure 7b

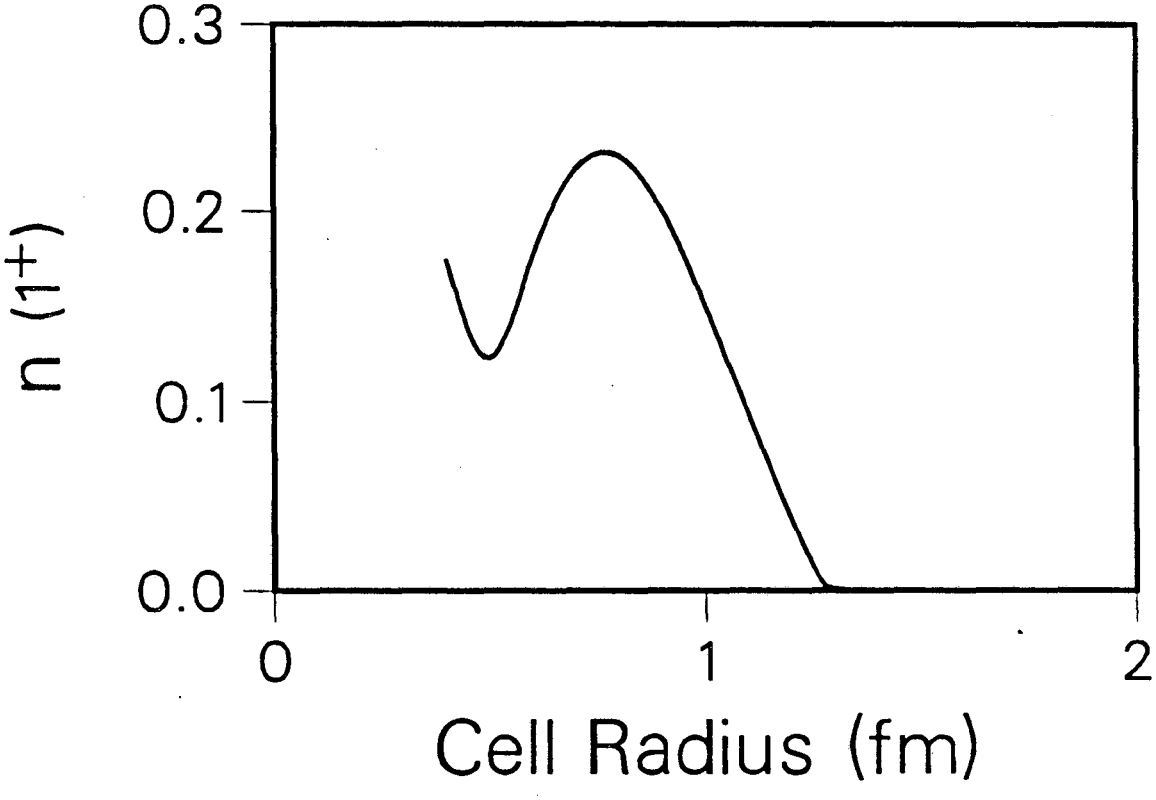

Figure 8

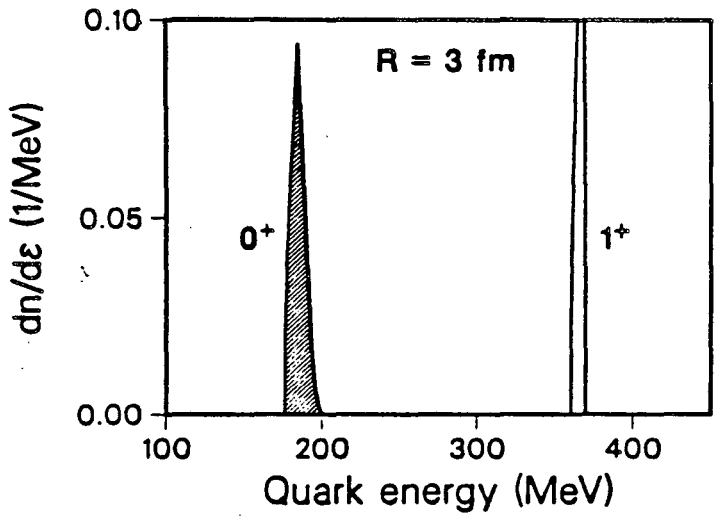

Figure 9a

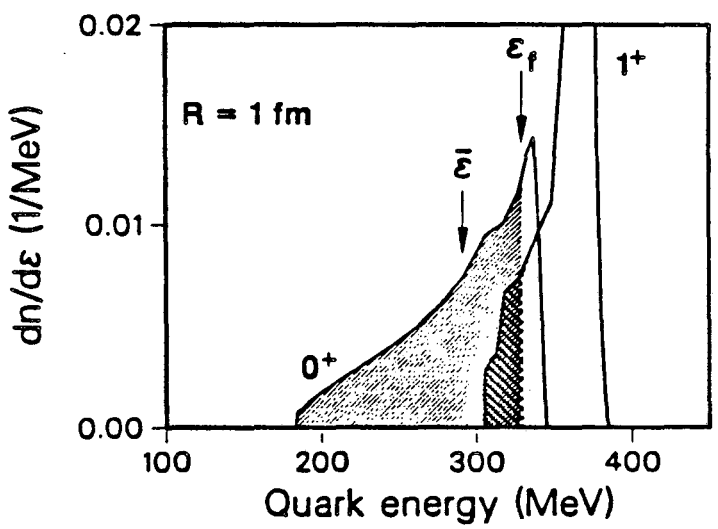

Figure 9b

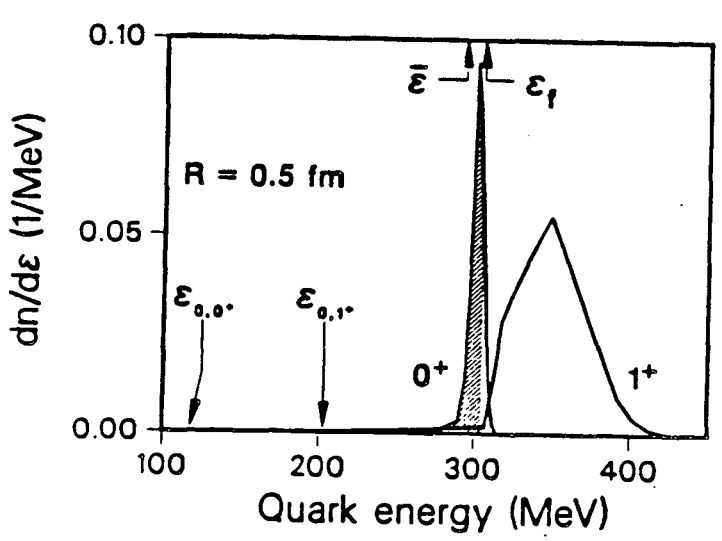

Figure 9c

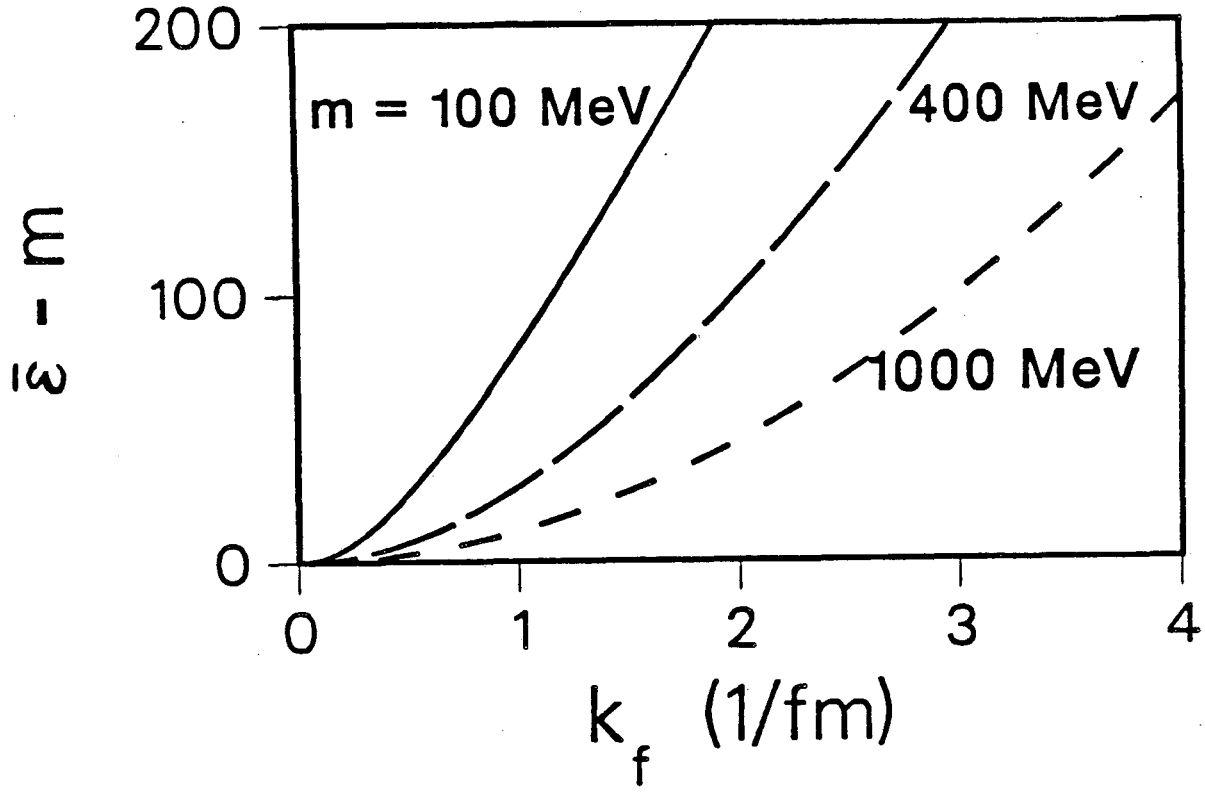

Figure 10a

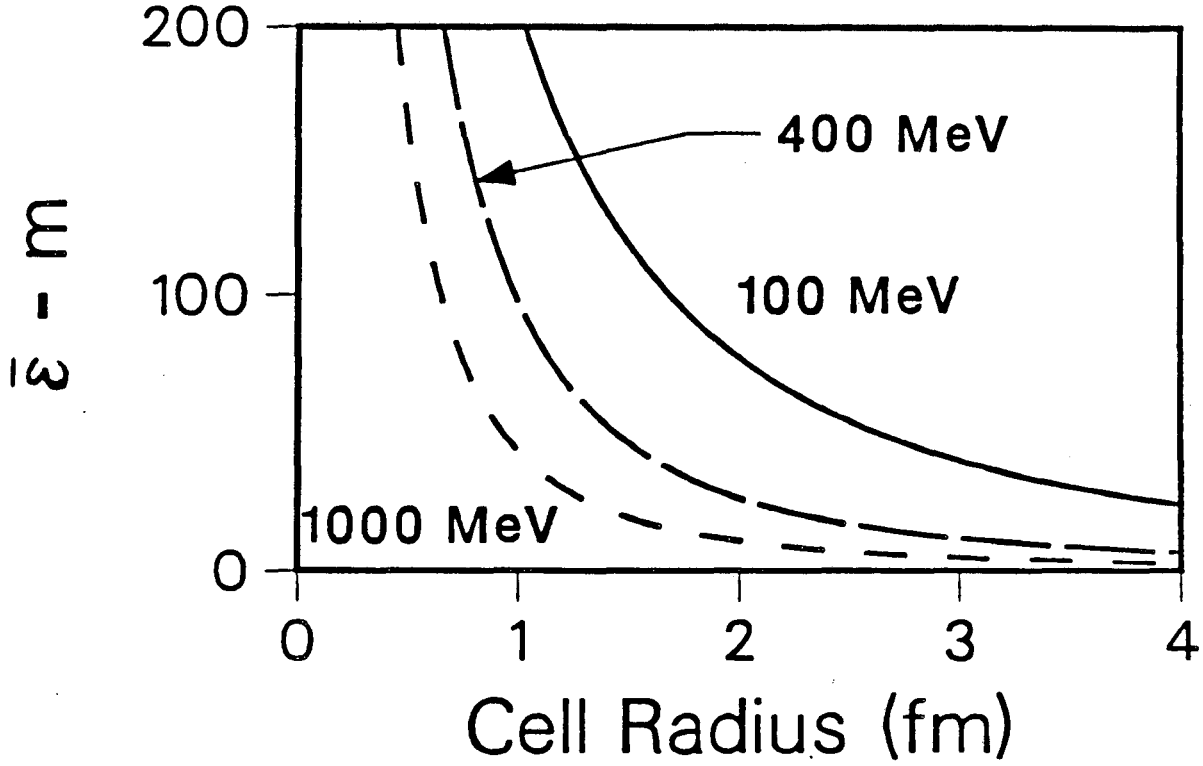

Figure 10b

This report was done with support from the Department of Energy. Any conclusions or opinions expressed in this report represent solely those of the author(s) and not necessarily those of The Regents of the University of California, the Lawrence Berkeley Laboratory or the Department of Energy.

Reference to a company or product name does not imply approval or recommendation of the product by the University of California or the U.S. Department of Energy to the exclusion of others that may be suitable.

LAWRENCE BERKELEY LABORATORY
TECHNICAL INFORMATION DEPARTMENT
UNIVERSITY OF CALIFORNIA
BERKELEY, CALIFORNIA 94720